Communication

Calcium Sensor for Photoacoustic Imaging

Sheryl Roberts, Markus Seeger, Yuanyuan Jiang, Anurag Mishra, Felix Sigmund, Anja Stelzl, Antonella Lauri, Panagiotis Symvoulidis, Hannes Rolbieski, Matthias Preller, Xosé Luís Deán Ben, Daniel Razansky, Tanja Orschmann, Sabrina Desbordes, Paul Vetschera, Thorsten Bach, Vasilis Ntziachristos, and Gil Gregor Westmeyer

J. Am. Chem. Soc., **Just Accepted Manuscript** • DOI: 10.1021/jacs.7b03064 • Publication Date (Web): 25 Sep 2017

	Razansky, Daniel; Helmholtz Zentrum München (GmbH), Institute of Biological and Medical Imaging Orschmann, Tanja; Helmholtz Zentrum Munchen Deutsches Forschungszentrum fur Umwelt und Gesundheit, Institute of Developmental Genetics Desbordes, Sabrina; Helmholtz Zentrum Munchen Deutsches Forschungszentrum fur Umwelt und Gesundheit, Institute of Developmental Genetics Vetschera, Paul; Helmholtz Zentrum Munchen Deutsches Forschungszentrum fur Umwelt und Gesundheit Bach, Thorsten; Technische Universitaet Muenchen, Lehrstuhl fuer Organische Chemie I Ntziachristos, Vasilis ; Technische Universität München & Helmholtz Zentrum München, Chair of Biological Imaging Westmeyer, Gil; Technical University of Munich (TUM), Nuclear Medicine; Helmholtz Zentrum Munchen Deutsches Forschungszentrum fur Umwelt und Gesundheit, Institute for Biological and Medical Imaging ; Helmholtz Zentrum Munchen Deutsches Forschungszentrum fur Umwelt und Gesundheit, Institute of Developmental Genetics

Calcium Sensor for Photoacoustic Imaging

Sheryl Roberts[†‡¥], Markus Seeger[§‡], Yuanyuan Jiang[‡¥], Anurag Mishra[‡¥], Felix Sigmund[‡¥], Anja Stelzl[‡¥], Antonella Lauri[†‡¥], Panagiotis Symvoulidis[†‡], Hannes Rolbieski, Matthias Preller[◊], X. Luís Deán-Ben[‡], Daniel Razansky[‡], Tanja Orschmann[◊], Sabrina Desbordes[◊], Paul Vetschera[§], Thorsten Bach[Ψ], Vasilis Ntziachristos[§‡], and Gil G. Westmeyer[†‡¥]

[†] Department of Nuclear Medicine, Technical University of Munich (TUM), Ismaninger Str. 22, 81675 Munich, Germany.
[‡] Institute for Biological and Medical Imaging & [¥]Institute of Developmental Genetics, Helmholtz Zentrum München, Ingolstädter Landstraße 1, 85764 Oberschleißheim, Germany.
[◊] Institute for Biophysical Chemistry, Carl-Neuberg-Straße 1, Hannover Medical School, 30625 Hannover.
[§] Chair for Biological Imaging, Technical University of Munich (TUM), Trogerstr. 9, 81675 Munich, Germany.
[Ψ] Chair of Organic Chemistry I, Technical University of Munich (TUM), Lichtenbergstraße 4, 85747 Garching, Germany.

Supporting Information

ABSTRACT: We introduce a selective and cell-permeable Calcium (Ca^{2+}) Sensor for Photoacoustics (CaSPA) which is a versatile imaging technique that allows for fast volumetric mapping of photoabsorbing molecules with deep tissue penetration. To optimize for Ca^{2+}-dependent photoacoustic signal changes, we synthesized a selective metallochromic sensor with high extinction coefficient, a low quantum yield, and high photobleaching resistance. Micromolar concentrations of Ca^{2+} lead to a robust blueshift of the absorbance of CaSPA which translated into an accompanying decrease of the peak photoacoustic signal. The acetoxymethyl esterified sensor variant was readily taken up by cells without toxic effects and thus allowed us for the first time to perform live imaging of Ca^{2+} fluxes in genetically unmodified cells, tissue culture as well as in zebrafish larval brain *via* combined fluorescence and photoacoustic imaging.

■ INTRODUCTION

Calcium (Ca^{2+}) is a key second messenger controlling *e.g.* contractility in heart and skeletal muscle and triggering secretory processes in immune, neuroendocrine, and neuronal cells.[1] It is thus of great interest to map spatiotemporal patterns of Ca^{2+}-signaling across whole organs in intact animals. Photoacoustic imaging (PAI) is a technique with deep tissue penetration that provides volumetric information on the distribution of photoabsorbers with ultrasound resolution.[2] This performance is made possible by exploiting the photoacoustic effect which describes the radiationless conversion of electromagnetic energy into mechanical energy occurring when chromophores thermoelastically expand upon photoabsorption. The resulting mechanical waves propagate through the surrounding tissue and can be detected via ultrasound transducers such that imaging volumes can be reconstructed. The key advantages of PAI are therefore that its resolution is insensitive to photon scattering and that it can provide volumetric information with high frame rates, because scanning procedures are not necessary.[3]

PAI readily detects hemodynamics and can indirectly localize brain activity because neuronal activity is correlated with vasodilation in mammalian brains (neurovascular coupling).[3] However, molecular signals that are directly linked to neuronal activity, such as intracellular calcium transients, could so far not be effectively read out by PAI due to a lack of appropriate molecular sensors.

In distinction to fluorescence imaging, the ideal photophysical properties of a chromophore optimized for photoacoustic detection are a low quantum yield (QY) and a high molar extinction coefficient (ε), as well as high photobleaching resistance. To design a reversible sensor for photoacoustics based on these prerequisites, one may search for functionalizations that alter ε and/or QY as a function of the analyte concentration or environmental parameter of interest. A photoacoustic sensor for Ca^{2+} should furthermore be highly selective for the target analyte over other biologically important divalent metals, in particular magnesium (Mg^{2+}) which is present at much higher intracellular concentrations.[4] Selectivity against zinc (Zn^{2+}) is also desirable, as Zn^{2+} is known to be colocalized with glutamate in neurons[5] and co-packaged with insulin in vesicles that are released from beta cells in a Ca^{2+}-dependent manner.[6] Furthermore, transmembrane delivery of the Ca^{2+} sensor should be efficient in order to load the majority of cells in a PAI voxel and thereby minimize partial volume effects. This set of specifications is however not fulfilled by most current calcium sensors used for fluorescence microscopy as those fluorophores, such as Oregon Green BAPTA-1 operate mainly by a change in QY.[7] Some well-known chromophores that change their absorbance in response to metal binding (metallochromic substances), such as Arsenazo III and Chlorophosphonazo III, exhibit specific absorbance changes in response to Ca^{2+}.[8] However, these compounds have a lower selectivity for Ca^{2+} as compared with BAPTA while forming complexes with two dye molecules per Ca^{2+}. Furthermore, the negatively charged Ca^{2+}-binding moieties of these dyes cannot be easily modified to achieve efficient delivery into cells.[9] Photoacoustic signals were measured from Arsenazo III packaged into liposomes and recently also from cells into which the highly concentrated compound was loaded, however resulting in measurable toxicity [10,11] as expected from arsenazo dyes.[12] Recently, a Cu^{2+}-responsive probe for photoacoustic detection was reported based on the Cu^{2+}-triggered cleavage of a 2-picolinic ester bond that led to a change of the photoacoustic spectrum. However, this detection mechanism is not reversible.[13]

To provide the first cell-permeable and selective Ca^{2+}-sensor for photoacoustics (CaSPA), we thus focused on metallochromic compounds that undergo a photoinduced charge transfer (PCT) as described for fura-2[14], in which a Ca^{2+} sensitive donor (aniline in BAPTA) is conjugated to an acceptor molecule in the fluorophore (amino group) leading to a spectral blueshift upon calcium binding.[15,16] We therefore reasoned that replacing the chromophore in fura-2 with a semi-cyanine chromophore could maintain the PCT mechanism but shifted to longer wavelengths more suitable for photoacoustics.

■ RESULTS AND DISCUSSION

We here demonstrate the result of this design strategy, a new metallochromic Ca^{2+}-Sensor for Photoacoustics (CaSPA), which is highly selective for Ca^{2+} - virtue of its BAPTA chelation group - and is readily cell permeable in its acetomethoxy ester (AM) form.

Figure 1 schematizes the chemical structure of the CaSPA_550 chromophore in its unbound (left) and Ca^{2+}-bound form (right, Figure 1a). The semi-cyanine chromophore of CaSPA_550 (**5,** Figure S1a in the Supporting Information) was synthesized via a condensation reaction between 3-ethyl-1,1,2-trimethyl-1H-benzo[e]indol-3-ium iodide, containing an activated methyl group and the appropriate aldehyde of 1,2-bis(2-

aminophenoxy)ethane N,N,N',N'-tetraacetate skeleton resulting in deep purple crystals with 85% yield. Subsequent demethylation using NaOH (aq) was carried out at room temperature and the resulting product was dried under high vacuum to obtain the corresponding free acid in low yields (≤ 5%). To improve the yield, saponification of the methyl ester groups was performed with tetrabutylammonium hydroxide (yield of up to 20%), which increased the solubility of the acid in polar organic solvents for further esterification reaction. The resulting product dried *in vacuo* is colorless in organic solvents and its deep purple color is only observed under polar conditions. Further esterification of **(5)** was carried out by dissolving the free acid with five equivalents of DIPEA and six equivalents of acetoxymethyl (AM) bromide in acetonitrile. Purification yielded purple crystals of CaSPA_550-AM (Figure S1 in the Supporting Information).

Photophysical characterization of CaSPA_550 in the absence of Ca^{2+}, revealed an absorption spectrum with a prominent peak at 550 nm with ϵ_{550} = 77,745 M^{-1} cm^{-1}. As a function of increasing Ca^{2+} concentrations (0-39 µM), CasPA_550 exhibited a reduction of its peak absorbance at 550 nm and the appearance of a minor blueshifted absorbance peak at 455 nm. The resulting maximum signal decrease at 550 nm was ~50%; the amplitude change at 455 nm was ~65% (Figure 1b, Figure S2).

In addition, an isosbestic point at 470 nm was apparent that could be used for ratiometric measurements correcting for differences in concentrations of the sensor (Figure S3). Absorbance of CaSPA_550 was not strongly affected by lowering pH to values that may be present in endosomes and synaptic vesicles but showed a blueshift and drop in absorbance when the pH was lowered to very acidic (pH 3.1) values (Figure S4). The peak fluorescence emission measured at 634 nm also decreased to half of the intensity as a function of increasing concentrations of Ca^{2+} (Figure 1c). However, we observed no change in QY upon binding of Ca^{2+}, which was low as desired for photoacoustics (an absolute measurement gave: QY_{noCa2+}= 0.01; $QY_{39\mu MCa2+}$= 0.009; a relative measurement against rhodamine 101 yielded: QY_{noCa2+}= 0.007 ± 0.0003; $QY_{39\mu MCa2+}$= 0.008± 0.0008).

We subsequently measured the photoacoustic spectra of the identical samples on a custom-built photoacoustic spectrometer (see Experimental Section in the Supporting Information) and observed that the peak photoacoustic signal at 550 nm also decreased by a factor of about two in response to 39 µM of Ca^{2+} (Figure 1d). The changes of the peak intensities of the absorbance spectra were significantly correlated with the changes of the peak photoacoustic signal (R^2 = 0.99); the peak fluorescence signal followed the changes in the absorbance (R^2 = 0.99).

To gain insights into the mechanism of photophysical changes upon Ca^{2+} binding, we performed quantum chemical calculations of ground and excited electronic states of CaSPA_550 using density functional theory (DFT) and time-dependent DFT (TD-DFT) with the M06-2X hybrid exchange-correlation functional and the M6-31(TM)** basis set. The computed vertical absorption energies for the uncomplexed and Ca^{2+}-bound CaSPA_550 are 2.48 eV and 2.92 eV, respectively, corresponding to vertical transition wavelengths of 500 nm (-Ca^{2+}) and 425 nm (+Ca^{2+}) (Figure S5 and Table S1). Therefore, our TD-DFT calculations predict a marked blue shift upon Ca^{2+} complexation, which is in line with the observed hypsochromic shift of the absorption band.

We determined the K_D values for calcium to be ~4 µM (Figure 2a and Figure S3); The selectivity for Ca^{2+} over Mg^{2+}, Zn^{2+}, and Cu^{2+} was high as expected from BAPTA as none of these metals induced any reduction in the absorbance (Figure 2b, Figure S6). Furthermore, the compound proved to be very photobleaching resistant (Figure S7).

Encouraged by the favorable photophysical properties of CaSPA_550, we next sought to test the calcium sensor in cells. To render the molecule cell-permeable, we generated the acetoxymethyl ester variant CaSPA_550-AM [17] which we found to be spectrally different from CaSPA_550 with a peak absorbance at ~590 nm (ϵ_{590} = 116,500 M^{-1} cm^{-1}) and a peak fluorescence amplitude at ~606 nm. Esterification also ensured that the absorbance and fluorescence spectra were unaltered in the presense of high concentrations (1 mM) of Ca^{2+} or Mg^{2+} (Figure S8).

We found that CaSPA_550-AM was taken up by Chinese Hamster Ovary Cells (CHO) as well as Human Embryonic Kidney Cells (HEK 293) after incubation with low micromolar concentrations without affecting cell viability (Figures S9, S10, S11).

Figure 3a shows fluorescence signal trajectories obtained from CaSPA_550 loaded CHO cells in which calcium influx was

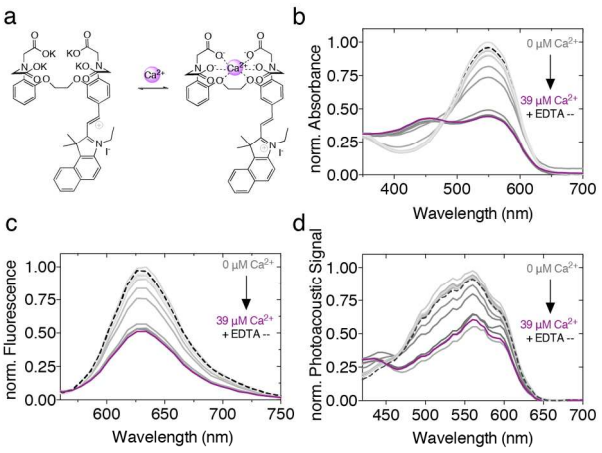

Figure 1. Photophysical characterization of CaSPA_550 in response to Ca^{2+} ions. (**a**) Chemical structure of CaSPA_550 in its unbound (left) and Ca^{2+}-bound (right) form (**b-d**) Spectroscopic analysis of CaSPa_550 (25 µM) dissolved in MOPS (2 mM) buffer containing increasing concentrations of free Ca^{2+} (0-39 µM). Spectra were obtained for (**b**) absorbance, (**c**) fluorescence, and (**d**) photoacoustic readout. Addition of 10 mM of the tight chelator EDTA competes out Ca^{2+} from CasPA_550 and reverts the signal amplitudes (dashed line in b,c,d).

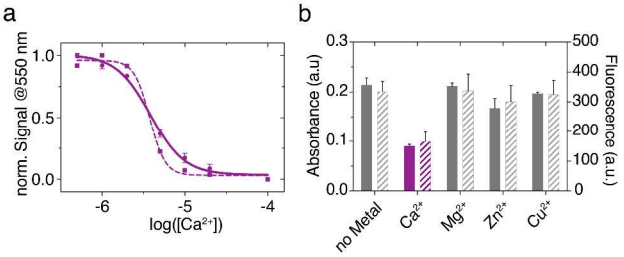

Figure 2. Sensitivity and selectivity of CaSPA_550 for Ca^{2+}. (a) The dissociation constant (K_D) for Ca^{2+} binding was determined by photoacoustics (3.9 µM; 95% Confidence Interval (CI): 2.9- 5 µM) absorbance (4.0 µM; 95% CI: 3.2- 4.9 µM). **(b)** Selectivity of the sensor was tested by plotting the peak of the absorbance (filled bars) and fluorescence spectra (striped bars) for several divalent metals added at 50 µM to 30 mM MOPS (3-(N-morpholino)propanesulfonic acid) containing also 100 mM KCl. Each data point is the mean of 3 experiments with error bars representing the standard error of the mean (SEM).

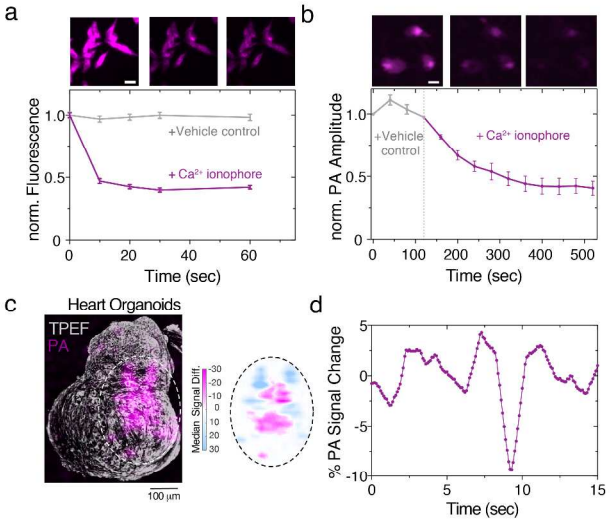

Figure 3. Imaging of calcium fluxes in cells and heart organoids by CaSPA_550 AM. (a) Fluorescence signal trajectories of CHO cells incubated with CaSPA_550 (2 µM, 30 minutes) in response to Ca^{2+} influx triggered by addition of a Ca^{2+} ionophore (Br-A23187, 10 µM in HBSS with Ca^{2+} and Mg^{2+}). Insets show fluorescence images obtained at the time points indicated. Vehicle control was 0.5% DMSO. The average fluorescence intensities were extracted by manual segmentation and plotted normalized to the fluorescence intensity of each cellular ROI before addition of the ionophore or vehicle control (error bars represent the standard error of the mean (SEM)). (b) Analogous experiment conducted with optical resolution photoacoustic microscopy (OR-PAM) in HEK cells. Photoacoustic signal time courses were recorded after addition of vehicle control (0.5% DMSO) followed by Ca^{2+} ionophore (Br-A23187, 10 µM). The insets (a,b) show exemplary FOVs (at 0, 10 and 20 sec in (a), and 0, 200 and 440 sec in (b) with scale bars representing 20 µm (a) and 10 µm (b). (c) Heart organoids loaded with CaSPA_550-AM and visualized as co-registered overlay of maximum amplitude projections of the OR-PAM image time series (magenta) and two-photon excitation fluorescence volume (TPEF) (gray). The median signal differences of the time series are shown on the map to the right. (d) Corresponding PA signal time course averaged over the region of interest (ROI) indicated with dashed lines in (c).

triggered by a calcium-specific ionophore (Br-A23187) which lead to a ~50% signal decrease as compared to vehicle control. Corresponding data from HEK cells are shown in Figure S11. We then conducted corresponding experiments on a custom-built hybrid 2-photon and optical resolution photoacoustic microscope (OR-PAM) that achieves ~1 µm axial and ~5 µm lateral resolution.[18,19] As can be seen in Figure 3b, CaSPA_550-loaded cells generated robust photoacoustic contrast that decreased to ~50% after addition of the Ca^{2+} ionophore.

These substantial signal changes in cell experiments prompted us to subsequently test the photoacoustic sensor in three-dimensional tissue culture. For this purpose, we cultured heart organoids, which spontaneously generate Ca^{2+} transients, and loaded them with CaSPA_500-AM. Via epifluorescence microscopy, we could observe fluorescent signal reductions throughout a large stationary region of interest (ROI) that were time-locked to small contractions detectable on the outer ring of the organoid (gray shaded time intervals in Figure S12a) as expected for a Ca^{2+} response of the weakly fluorescent metallochromic sensor. Conversely, when we loaded organoids with the commonly used green fluorescent calcium indicator Fluo-4-AM, we observed increases of the fluorescent signal associated with small contractions detected at the outer rim of the heart tissue (gray shaded bars in Figure S12b).

Figure 3c displays the maximum amplitude projections of the optoacoustic volumes from CaSPA-loaded heart organoids (magenta) overlaid on the fluorescence signals from two-photon excitation (gray) revealing the structure of the organoid. When we sampled at the maximum photoacoustic imaging frame rate of 1 Hz, we observed photoacoustic signal reductions in the ROI of up to 10% in a freqency range that we also observed with the standard Fluo-4-AM in fluorescence microscopy at a comparable sampling rate (Figure 3d, S12b).

Next, we sought to work with the CaSPA_550-AM sensor *in vivo* and thus delivered it to zebrafish larval brains. We observed that the compound spread out well from the intraventricular injection point, and was taken up by cells (white arrow in Figure S13a,a'). We then embedded a CaSPA-injected zebrafish larva next to a non-injected control fish in agar and positioned it in a multispectral photoacoustic imaging device. This imaging system is capable of fast acquistion of photoacoustic spectra in imaging volumes over time via the use of a tunable laser. In addition to the photoacoustic signal time courses, we also recorded

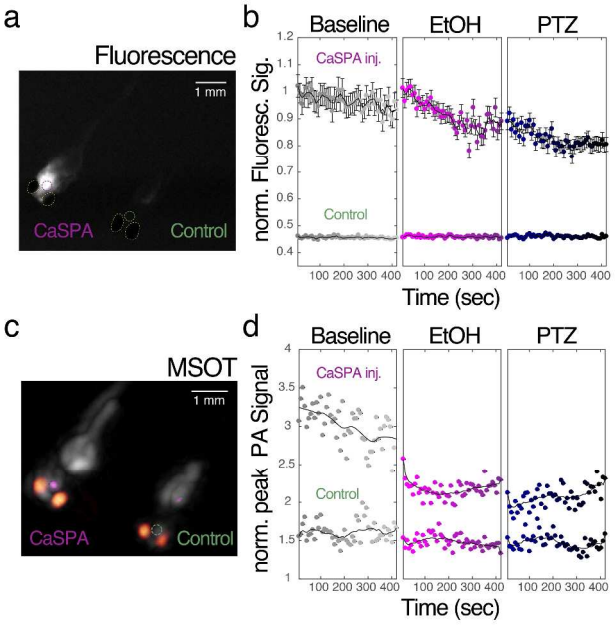

Figure 4. Combined multispectral photoacoustic tomography and fluorescence imaging of CaSPA-injected larval zebrafish brain. (a) Single imaging frame of the epifluorescence time series showing fluorescence signal of the brain ROI of the CaSPA_550 AM-injected zebrafish (550 nm excitation, absorbing eyes highlighted with dashed lines) as well as the non-injected control. (b) Corresponding fluorescence signal time course of an ROI placed over the peak fluorescence (circle with magenta broken lines) during 7 minute baseline recording followed by two additional 7 minute measurements after stimulations with the nuerostimulatns ethanol (EtOH) and pentylenetetrazole (PTZ). The fluorescence signal time course (errobars represent SEM) of the corresponding brain region in the non-injected control fish is shown in green. (c) Simultanously acquired photacoustic imaging data with 50 photoacoustics spectra (430-630 nm) obtained in each observational block. The magenta overlay represents the voxel time courses during the baseline recording that matched the CaSPA-550 spectrum. The melanin containing eyes which give a broad PA spectrum are overlaid in orange. An anatomical reference is shown in gray (d) Corresponding time courses of the normalized peak photoacoustic signal during baseline and after stimulation with EtOH and PTZ. The signal trajectory of the control fish is shown on the bottom. Errorbars represent SEM and may be smaller than the symbols.

fluorescence signal changes with a camera mounted on the opposite side from the photacoustic sensor array. As displayed in Figure 4a, the brain of the CaSPA-injected fish showed a strong fluorescent signal (excitation at 550 nm) over 7 minutes of baseline observation, whereas no fluorescent signal was detected from the brain of the control fish. When we applied a low concentration of ethanol (1% in fish water [20]), a neurostimulant with fast cellular diffusion, to both agar-embedded fish, we observed a signal decay and increased signal fluctuations (Figure 4b). Subsequently we superfused the potent neurostimulant pentylenetetrazole (PTZ, 5 mM in fish water [21]) which is commonly used to induce strong Ca^{2+} signaling in the brain and observed an overall fluorescent signal decrease in the brain region of the CaSPA injected fish. Throughout the experiment, the autofluorescence signals from the swim bladders of both fish observed at shorter excitation wavelenghts remained constant (Figure S13b,b'b''). When we then analyzed the simultaneoulsy acquired photoacoustic data, we located the CaSPA_550 spectrum (Fig. S13c) at the location with strong fluorescence signal in the CaSPA-injected fish (Fig. 4c, magenta overlay). Over time, we observed a decrease of the photoacoustic signal peak around 550 nm during the stimulation with EtOH which slightly increased before further signal reduction after addition of PTZ (Figure 4d). The brain of the control fish generated only low signal around 550 nm and signal amplitudes obtained from the melanin containing eyes of both fish remained constant over time (Fig. 13d,d').

■ CONCLUSIONS

These experiments jointly demonstrate that the metallochromic Ca^{2+}-sensor for photoacoustics (CaSPA_550) which we introduce here is the first probe that possesses the necessary photophysical and biochemical properties to enable imaging of intracellular Ca^{2+} transients with photoacoustics in cells, organotypic tissue culture and *in vivo* in larval zebrafish brain. The semi-cyanine scaffold we chose may serve as a versatile platform to generate metallochromic sensors selective for other biologically relevant metals or small analytes to enable molecular and dynamic photoacoustic imaging with photo-scattering-independent resolution

■ ASSOCIATED CONTENT

Supporting Information.
Supporting Tables and Figures, as well as Experimental Methods. This material is available free of charge via the Internet at http://pubs.acs.org.

■ AUTHOR INFORMATION

Corresponding Author

* gil.westmeyer@tum.de

ORCID

Gil Gregor Westmeyer: **0000-0001-7224-8919**

Notes
The authors declare no competing financial interest.

■ ACKNOWLEDGEMENTS

We thank Dr. Robert Pal (Durham University) for relative QY measurements, Dr. Andreas Bauer (Technical University of Munich) for absolute QY measurements, and Christian Hundshammer for help with HPLC. We thank Prof. Dr. Oliver Plettenburg for helpful comments on the manuscript.

We are grateful for support from the Helmholtz Alliance ICEMED (AM, GGW), the European Research Council under grant agreements ERC-StG: 311552 (GGW), the Priority program SP1665 of the German Research Foundation (DFG), as well as the Laura Bassi Award of TUM (SR), grant agreements CRC 1123 (Z1), and Reinhard Koselleck project (NT 3/9-1).

■ REFERENCES

(1) Berridge, M. J.; Bootman, M. D.; Roderick, H. L. *Nat Rev Mol Cell Biol* **2003**, *4* (7), 517.
(2) Taruttis, A.; Ntziachristos, V. *Nature Photon* **2015**, *9* (4), 219.
(3) Gottschalk, S.; Fehm, T. F.; Deán-Ben, X. L.; Razansky, D. *J Cereb Blood Flow Metab* **2015**.
(4) Li Smerin, Y.; Levitan, E. S.; Johnson, J. W. *The Journal of Physiology* **2001**, *533* (3), 729.
(5) Kalappa, B. I.; Anderson, C. T.; Goldberg, J. M.; Lippard, S. J.; Tzounopoulos, T. *Proceedings of the National Academy of Sciences* **2015**, 201512296.
(6) Li, Y. V. *Endocrine* **2014**, *45* (2), 178.
(7) Wilms, C. D.; Eilers, J. *J Microsc* **2007**, *225* (3), 209.
(8) Durham, A. C. H.; Walton, J. M. *Cell Calcium* **1983**, *4* (1), 47.
(9) Thomas, M. V. *Biophys. J.* **1979**, *25* (3), 541.
(10) Cooley, E. J.; Kruizinga, P.; Branch, D. W.; Emelianov, S. Achilefu, S., Raghavachari, R., Eds.; SPIE, 2010; Vol. 7576, p 75761J.
(11) Dana, N.; Fowler, R. A.; Allen, A.; Zoldan, J.; Suggs, L.; Emelianov, S. *Laser Phys. Lett.* **2016**, 1.
(12) Baylor, S. M.; Hollingworth, S.; Hui, C. S.; Quinta-Ferreira, M. E. *The Journal of Physiology* **1986**, *377* (1), 89.
(13) Li, H.; Zhang, P.; Smaga, L. P.; Hoffman, R. A.; Chan, J. *J Am Chem Soc* **2015**, *137* (50), 15628.
(14) Grynkiewicz, G.; Poenie, M.; Tsien, R. Y. *Journal of Biological Chemistry* **1985**, *260* (6), 3440.
(15) Valeur, B. *Coordination Chemistry Reviews* **2000**, *205* (1), 3.
(16) Oheim, M.; van 't Hoff, M.; Feltz, A.; Zamaleeva, A.; Mallet, J.-M.; Collot, M. *Biochim. Biophys. Acta* **2014**, *1843* (10), 2284.
(17) Tsien, R. Y. *Nature* **1981**, *290* (5806), 527.
(18) Seeger, M.; Karlas, A.; Soliman, D.; Pelisek, J.; Ntziachristos, V. *Photoacoustics* **2016**.
(19) Soliman, D.; Tserevelakis, G. J.; Omar, M.; Ntziachristos, V. *Sci Rep* **2015**, *5*, 12902.
(20) Ikeda, H.; Delargy, A. H.; Yokogawa, T.; Urban, J. M.; Burgess, H. A.; Ono, F. *Plos One* **2013**, *8* (5), e63318.
(21) Randlett, O.; Wee, C. L.; Naumann, E. A.; Nnaemeka, O.; Schoppik, D.; Fitzgerald, J. E.; Portugues, R.; Lacoste, A. M. B.; Riegler, C.; Engert, F.; Schier, A. F. *Nat. Methods* **2015**, *12* (11), 1039.

Keywords: Imaging agents • Photoacoustic Imaging • Optoacoustic Imaging • metallochromic agent • calcium imaging

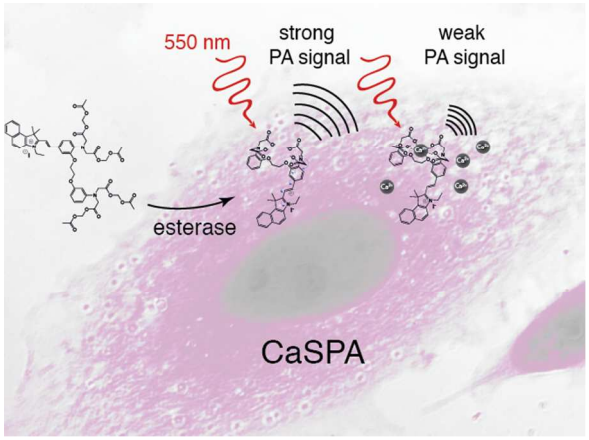
550 nm
strong
PA signal
weak
PA signal
esterase
CaSPA